Draft version July 30, 2018
Typeset using LaTeX **twocolumn** style in AASTeX62

Revised Simulations of the Planetary Nebulae Luminosity Function

Lucas M. Valenzuela[1] and Roberto H. Méndez[2]

[1] *Fakultät für Physik, Ludwig-Maximilians-Universität, Schellingstraße 4, 80799 München, Germany*
[2] *Institute for Astronomy, University of Hawaii, 2680 Woodlawn Drive, Honolulu, HI 96822, USA*

Abstract

We describe a revised procedure for the numerical simulation of planetary nebulae luminosity functions (PNLF), improving on previous work (Méndez & Soffner 1997). The procedure now is based on new H-burning post-AGB evolutionary tracks (Miller Bertolami 2016). For a given stellar mass, the new central stars are more luminous and evolve faster. We have slightly changed the distribution of the [O III] 5007 intensities relative to those of Hβ and the generation of absorbing factors, while still basing their numerical modeling on empirical information extracted from studies of Galactic planetary nebulae (PNs) and their central stars. We argue that the assumption of PNs being completely optically thick to H-ionizing photons leads to conflicts with observations and show that it is necessary to account for optically thin PNs. Even allowing for this partial leaking of ionizing photons, as a result of the revised PNLF simulations we confirm that the observed PNLFs can be fitted using a maximum final mass that is much closer to the expected value for old stellar populations, significantly reducing a long-standing discrepancy between observed PNLFs and previous theoretical expectations. By adjusting the range of minimum to maximum final mass, it is also possible to explain the observed variety of PNLF shapes at intermediate magnitudes. The new PN formation rates are calculated to be slightly lower than suggested by previous simulations based on older post-AGB evolutionary tracks.

Keywords: galaxies: distances and redshifts — galaxies: individual (M 31, NGC 4697, M 60, LMC) — methods: numerical — planetary nebulae: general — stars: AGB and post-AGB

1. INTRODUCTION

If we can measure the nebular emission line fluxes of [O III] 5007 for many planetary nebulae (PNs) in a galaxy and transform the fluxes into apparent magnitudes $m(5007)$ (Jacoby magnitudes, defined by Jacoby (1989)), then we can build the planetary nebulae luminosity function (PNLF). It indicates how many PNs have [O III] 5007 at each apparent magnitude $m(5007)$. Empirically, it was discovered that the brightest PNs in a galaxy have similar absolute magnitudes $M(5007)$. This led to the suggestion of a universal bright end of the PNLF that could be used as a standard candle (Jacoby 1989). The PNLF has been used to determine extragalactic distances for almost 30 years now (beginning with Jacoby 1989; Ciardullo et al. 1989) and has proven to be a reliable distance indicator (see e.g. Ciardullo 2012).

The PNLF not only gives insight into the distance of a galaxy, but also into properties of the stellar population. Consider, for example, the PN populations of elliptical galaxies and of M 31's bulge. The bright ends of their observed PNLFs require the existence of very luminous central stars, approaching $7000\,L_\odot$ (see e.g. Jacoby & Ciardullo 1999; Méndez et al. 2005, 2008b). Until recently, this appeared to require very massive central stars (about $0.63\,M_\odot$), in strong disagreement with the expected maximum final mass of about $0.55\,M_\odot$ that would correspond to a turn-off initial mass of about $1\,M_\odot$ (Cummings 2017) in these rather old stellar populations.

This alarming discrepancy has now been drastically reduced by the introduction of new post-AGB evolutionary tracks by Miller Bertolami (2016). A modified luminosity–core mass relation has decreased the required central star mass from 0.63 to $0.58\,M_\odot$ (Méndez 2017), in much better agreement with theoretical expectations. The new tracks also show a much faster post-AGB evolution than previously calculated. This means that central stars of much lower mass than previously expected can produce visible PNs.

If we further assume that PNs are predominantly optically thick (opaque) to H-ionizing radiation from the central star (Gesicki et al. 2018), it becomes possible to produce a bright end of the PNLF which stays almost invariant for a variety of stellar population ages and star formation histories. This helps to understand the high quality of the PNLF as a standard candle.

However, there are good reasons to doubt that most PNs in a stellar population are completely optically thick. Looking around in our Milky Way we see PNs with predominantly bipolar symmetry, which means that they probably will start

leaking H-ionizing photons very soon, in directions where the nebular density is lower.

In view of this and other complications, PNLF simulations created using Monte Carlo techniques can be used to take a closer look at how sample size, population age, and partial absorption of ionizing photons affect the properties of the PNLF (Méndez et al. 1993; Méndez & Soffner 1997; Méndez et al. 2008b). The recent advances in post-AGB theory have induced us to revisit PNLF simulations.

In the present work we describe our revisions of the procedure outlined by Méndez & Soffner (1997) to generate PNLFs, using the new evolutionary tracks for low-mass stars (Miller Bertolami 2016) and a central star mass distribution derived from a modern DA white dwarf mass distribution (Kepler et al. 2017). The newly simulated PNLFs obtained in this way are compared with the observed PNLFs in a few selected galaxies to find out what the consequences of the new tracks are – on the shape and bright end of the PNLF, on the determination of the PN formation rate, and on the unresolved tension between PNLF distances and surface brightness fluctuation (SBF) distances (Ciardullo 2012; Méndez 2017).

2. CREATION OF EVOLUTIONARY TRACKS

Since the procedure closely follows the one described in Méndez & Soffner (1997), the reader may refer to that paper for more details. For brevity, here we will focus on the changes we have introduced. The evolutionary tracks of H-burning post-AGB stars are now taken from Miller Bertolami (2016). More specifically, we have selected five tracks corresponding to $Z_0 = 0.01$ from his Table 2, with initial masses of 1.0, 1.25, 1.5, 2.5, and 3.0 $M_\odot$. These tracks are based on improved models of AGB stars and evolutionary calculations. The main differences with previous work are that the new post-AGB stellar luminosities are higher and post-AGB timescales are shorter than what earlier models suggested.

As before, we have chosen to define the post-AGB age to be equal to the time passed since the moment the central star had a temperature of $T_{\rm eff} = 25\,000$ K. We will call the post-AGB ages just "ages" in what follows. Because the central star mass changes continuously with time, each track is assigned the average mass between the masses at ages 0 and 30 000 years. This hardly affects the outcome of the interpolated tracks since the change of mass along each track is much smaller than the central star mass itself, by an order of 10^{-4} to 10^{-5}.

We generated a look-up table similar to the one described in Méndez & Soffner (1997) to determine $\log T_{\rm eff}$ and $\log L$ as functions of 3000 ages between 0 and 30 000 years, and 260 masses between 0.530 and 0.706 solar masses. For the interpolations, the tracks were split up into three sections.

For the nearly horizontal heating tracks we used 40 temperatures between 25 000 and 81 000 K, at which we plotted $\log$ age and $\log L$ as functions of mass. To interpolate between the values given by the tracks, we fitted curves to these plots and calculated the age and luminosity for the 260 masses at each of the 40 temperatures.

For the white dwarf cooling tracks we used 60 luminosities between $\log L = 1.60$ and 2.75, at which we plotted $\log$ age and $\log T_{\rm eff}$ as functions of mass. We fitted curves to these plots and calculated the age and temperature for the 260 masses at each of the 60 luminosities.

For the curved section joining the heating and cooling tracks we used 90 lines radiating at different angles from a fixed point at $T_{\rm eff} = 81\,000$ K and $\log L = 2.75$. The values obtained at the intersections between these lines and the given tracks were used to plot $\log$ age, $\log T_{\rm eff}$ and $\log L$ as functions of mass. We then fitted curves to these plots to calculate age, temperature and luminosity for the 260 masses at each of these 90 angles.

Having 190 values of temperature and luminosity for each of the 260 masses along their respective tracks, we could interpolate between these to obtain $\log T_{\rm eff}$ and $\log L$ at 3000 ages between 0 and 30 000 years. The result was a look-up table that can be used to determine the temperature and luminosity of a star with a given age and mass by bivariate spline interpolation.

Figure 1 shows the evolutionary tracks for the five final (central star) masses used to calculate the interpolations.

3. GENERATION OF A PN POPULATION

When generating a sample of PN central stars, each star is assigned a random age and mass. The ages are uniformly distributed between 0 and 30 000 years – this is approximately the expected timescale of a PN, given typical expansion velocities and the largest observed PN sizes.

Because of the faster post-AGB evolution, central stars with lower masses than previously expected can produce visible PNs; but of course there must be a limit. PNs with central star masses below 0.53 $M_\odot$ should dissipate before the central stars can become hot enough to ionize the gas (see Figure 1). Therefore, we generated masses between 0.53 $M_\odot$ and a maximum final mass that we expected to be somewhere below 0.60 $M_\odot$. We approximated this range of masses as a linear distribution, with a mass of 0.58 $M_\odot$ being 2.5 times as likely as a mass of 0.53 $M_\odot$. This approximation for the central star mass distribution is based on the DA white dwarf mass distribution for $T_{\rm eff} \geq 13\,000$ K corrected by the $1/V_{\rm max}$ method in Kepler et al. (2017). We compare both mass distributions in Figure 2.

The HR diagram of 1500 PNs generated in this manner is shown in Figure 3. The values of central star temperature and

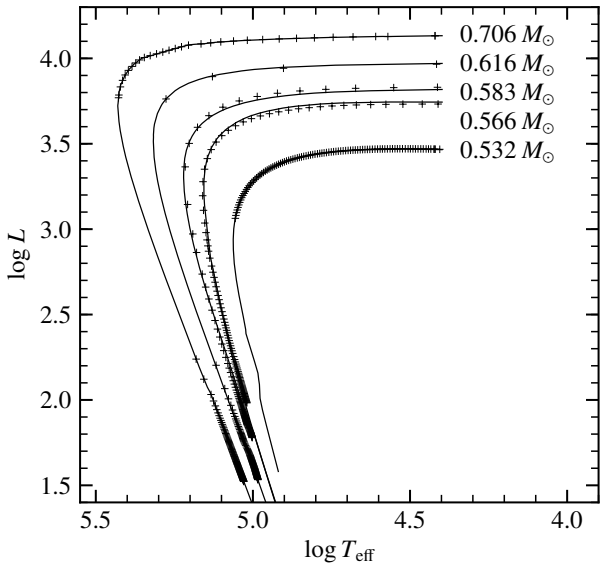

Figure 1. Solid lines show the five evolutionary tracks used to calculate our interpolations (Miller Bertolami 2016). Plus signs indicate the interpolated values of temperature and luminosity of central stars for the five masses at 100 evenly distributed ages between 0 and 30 000 years. There are an additional 30 values for the 0.706 $M_\odot$ track at 30 evenly distributed ages between 0 and 300 years. When comparing this figure with Fig. 1 in Méndez & Soffner (1997), note that the masses corresponding to a given luminosity are different, and that the post-AGB timescales of the new tracks are considerably shorter.

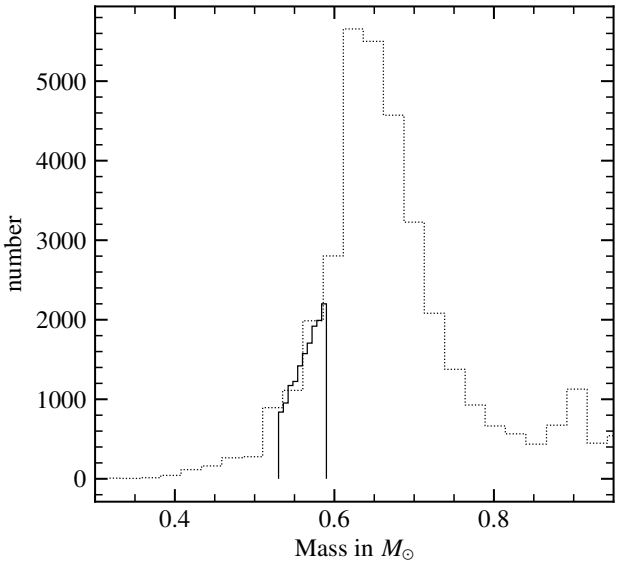

Figure 2. Histogram of 15 000 PNs (solid line) with central star masses between 0.53 and 0.59 $M_\odot$, compared with the DA white dwarf mass distribution from Kepler et al. (2017) (dotted line). The latter was scaled to match the chosen sample size in this mass range.

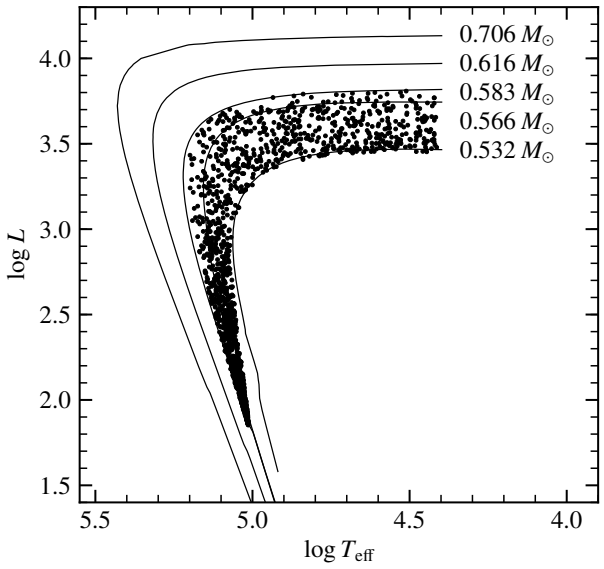

Figure 3. Solid lines show the same tracks for the five central star masses used in Figure 1. Dots indicate the values of temperature and luminosity of 1500 central stars with random ages and masses. The ages are generated from a uniform distribution between 0 and 30 000 years. The masses are generated in this case using a linear distribution between 0.53 and 0.58 solar masses, with a mass of 0.58 $M_\odot$ being 2.5 times as likely as a mass of 0.53 $M_\odot$.

luminosity were computed using the procedure described in Section 2.

4. ADJUSTMENTS TO THE [O III] 5007 RELATIVE INTENSITIES

To correct for the changes in mass distribution and evolutionary tracks, we adjusted the procedure that generates the λ5007 intensity, $I(5007)$, relative to the intensity of Hβ. We continued to compare our distribution to the one found in the LMC (using 118 PNs) and to the one found in the Milky Way (using 983 PNs). In both cases, we used the compiled data described in Section 4 of Méndez & Soffner (1997).

Our distribution is generated by following the previous procedure, with the following differences: We now use a Gaussian distribution centered at $I(5007) = 950$ on a scale of $I(\mathrm{H}\beta) = 100$ with FWHM = 375. We then lower the values above 1200 by up to 200 (values right above 1200 are only slightly decreased while values around 2000 are maximally decreased) to imitate the steeper drop-off on the right part of the distribution. We then cap the values at 1850. Because of the lower masses being used, we lower $I(5007)$ by 60 % for central stars with masses below 0.55 $M_\odot$ that are on heating tracks with $T_{\rm eff} > 75\,000$ K (instead of by 50 % for masses below 0.57 $M_\odot$). The new values were chosen to allow our generated distribution to fit the shapes of the observed ones

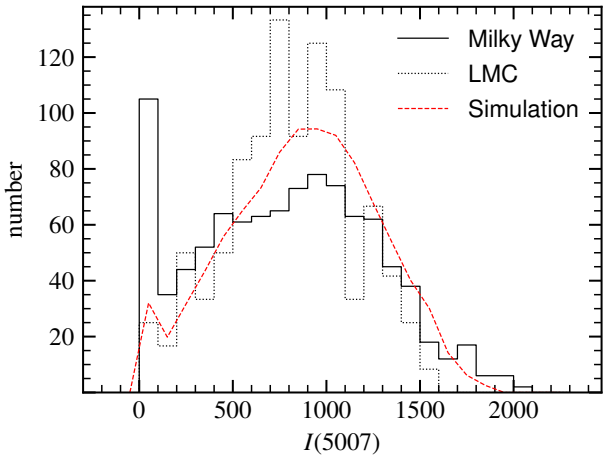

Figure 4. Our generated distribution of $I(5007)$ on a scale of $I(\mathrm{H}\beta) = 100$ compared with the observed distributions in the LMC (using 118 PNs) and the Milky Way (using 983 PNs). The histograms of our generated distribution and of the LMC have been normalized to the number of Milky Way objects.

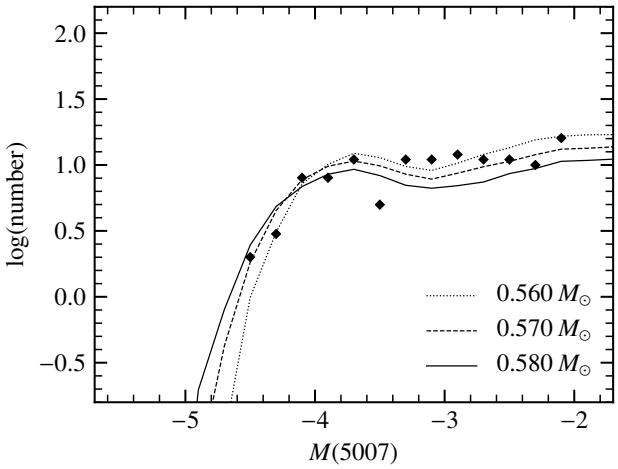

Figure 5. Statistically complete observed PNLF of M 31's bulge (using 119 PNs) from Ciardullo et al. (1989). We use a λ5007 extinction correction of 0.28 mag and a distance modulus of $m - M = 24.43$. The data are binned into 0.2 mag intervals. The observed PNLF (diamonds) is compared with simulated PNLFs using completely opaque PNs ($\mu = 1$ for all of them). The sample size for each simulated PNLF is 285 PNs. The simulations were run with three different mass ranges from 0.530 $M_\odot$ to the respective maximum final mass displayed at the bottom right.

in the LMC and the Milky Way as well as possible (see Figure 4).

5. THE NECESSITY OF THE ABSORBING FACTOR μ

In Méndez et al. (1992) an absorbing factor μ was introduced to describe the optical thickness of a nebula in the H Lyman continuum. Its value is equal to the fraction of ionizing stellar photons that are absorbed by the nebula, which means that $\mu = 1$ represents a completely optically thick or opaque PN, whereas a perfectly transparent PN has $\mu = 0$. A range of absorbing factors was used in PNLF simulations by Méndez & Soffner (1997).

Now that we were using new post-AGB tracks and a different central star mass range, we had to make sure whether this absorbing factor was still required by the simulation to reproduce observed PNLFs. We assumed for the following that all PNs are optically thick, that is, $\mu = 1$ for all of them. Having the temperatures, luminosities, and intensities of λ5007 relative to $I(\mathrm{H}\beta)$, we could generate a PNLF following the procedure described in Méndez & Soffner (1997).

For the observed data, we used a statistically complete PNLF with 119 PNs of M 31's bulge (samples A and B from Ciardullo et al. 1989). We transformed apparent into absolute λ5007 magnitudes adopting a distance modulus of $m - M = 24.43$ and an extinction correction for λ5007 of 0.28 mag, based on $E(B - V) = 0.08$.

At this point we introduced a quantity r that tells us how well a generated PNLF fits the observed one. We defined r to resemble the way the eye evaluates the fit in a plot. The sum of the squared deviations of $\log N$ seemed to be a good indicator. We used a histogram for $M(5007)$ between −6 and −2 with a bin size of 0.2 to match typical PNLFs found in the literature. Since numbers below $\log N = 0$ are much less relevant and because of $\lim_{N\to 0^+} \log N = -\infty$, we used $\log(0.5)$ instead of $\log N$ for values below $\log(0.5)$. We used this minimum value because $N < 0.5$ means that the probability of finding a PN in that particular bin is less than 50 %.

By adjusting the maximum final mass and the sample size in our simulated PNLFs, we found that a mass range of 0.530 to 0.570 solar masses and a sample size of 285 PNs gives the best fit to the observed PNLF of M 31 (see Figure 5).

Specifically, when calculating r for the three selected maximum final masses in Figure 5, we got 0.30 for 0.560 $M_\odot$, 0.20 for 0.570 $M_\odot$, and 0.37 for 0.580 $M_\odot$. Clearly, a maximum final mass of 0.570 solar masses gives us the best fit.

While the bright end can be fitted properly, the shape of the PNLF beyond $M(5007) = -3.5$ has a valley that does not match the observed PNLF particularly well. And, most importantly, the sample size of 285 PNs is too small if we compare it to 970, the total expected number of PNs in the region of M 31's bulge sampled by Ciardullo et al. (1989); see the discussion in their Section V.

If we now increase the sample size by a factor 3 to keep M 31's PNLF at the right distance, the simulated PNLF fails to fit. We conclude, as already stated by Méndez & Soffner (1997), that it is necessary to allow for PNs that leak ionizing photons from the central star. The empirical evidence for this is taken from Table 4 in Méndez et al. (1992), where we find a variety of μ values, from 1 to less than 0.1, and a clear trend of decreasing μ with increasing central star temperature.

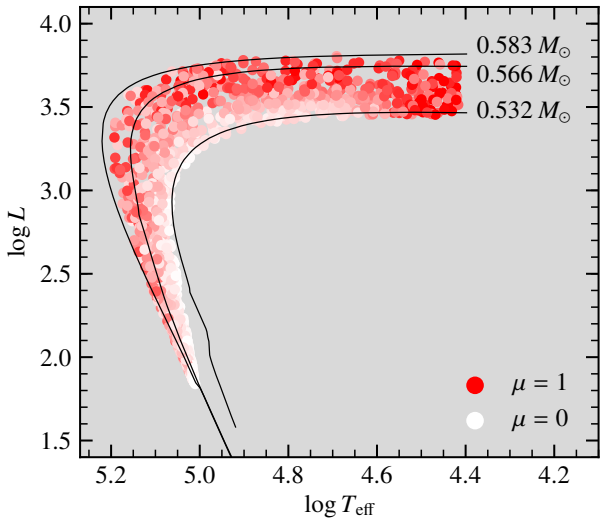

Figure 6. HR diagram showing the distribution of absorbing factor values in a sample of 1500 PNs that were generated with ages between 0 and 30 000 years and masses between 0.53 and 0.58 solar masses. The color lightness of each PN represents its absorbing factor μ, where red stands for $\mu = 1$ (optically thick) and white for $\mu = 0$ (completely transparent).

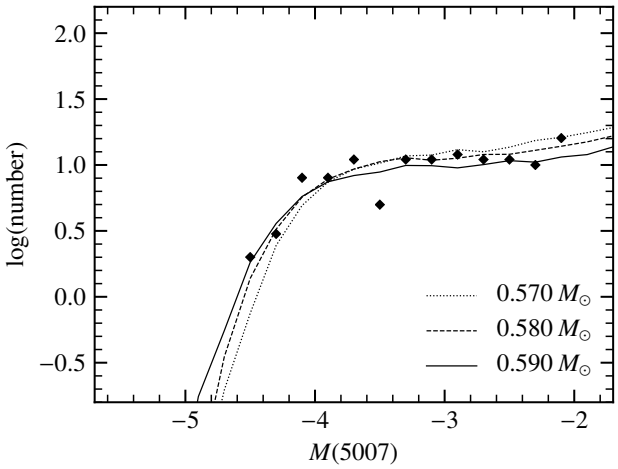

Figure 7. Statistically complete observed PNLF of M 31's bulge (diamonds, same data as in Figure 5), compared with simulated PNLFs using the absorbing factor distribution from Figure 6. The sample size for each simulated PNLF is 700 PNs. The simulations were run with three different mass ranges from 0.530 $M_\odot$ to the respective maximum final mass displayed at the bottom right.

As in previous work, we generated a distribution of μ values using random numbers. Further justification for this approach can be found in Section 2.4 of Méndez et al. (2008b). We implemented similar boundary conditions as Méndez et al. (1993) and Méndez & Soffner (1997): PNs at the beginning of the heating tracks tend to be more opaque and will become increasingly transparent at higher temperatures. For the slowly evolving low-mass central stars (see Figure 1), we expect the nebula to dissipate before reaching higher temperatures, so we assign low random absorbing factor values to them for higher ages. And finally, we use a similar method as Méndez & Soffner (1997) for generating decreasing μ-values for increasing ages on the cooling tracks, such that $\mu = 0$ for an age of 30 000 years. The resulting absorbing factor distribution in the HR diagram is shown in Figure 6.

6. ESTIMATING THE MAXIMUM FINAL MASS

Using the absorbing factor distribution from the previous section, we could again generate PNLFs for different maximum final masses. The best fit was found at a sample size of 700 and a maximum final mass of between 0.580 and 0.590 solar masses (see Figure 7). Again, we used the fitting parameter r defined in Section 5: We obtained 0.39 for 0.570 $M_\odot$, 0.18 for 0.580 $M_\odot$, and 0.14 for 0.590 $M_\odot$. This clearly gave us a better fit than when using completely opaque PNs ($r = 0.20$ for 0.570 $M_\odot$; see Figure 5). We omitted masses beyond 0.590 $M_\odot$ since the slopes of their PNLFs' bright ends do not match the observed one. Because of the distribution of absorbing factors, we required a much larger sample size. This is more reasonable for M 31's bulge and confirms that it is clearly preferable to allow for many optically thin PNs when simulating PNLFs.

Because of the small number of PNs surveyed by Ciardullo et al. (1989) in M 31's bulge, the uncertainty of the maximum final mass is high. For a better estimate of this value, we needed to consider an old stellar population with a larger sample size. For this purpose we used NGC 4697, a flattened elliptical galaxy in the Virgo southern extension. For the observed data, we used the method described in Méndez et al. (2001) to get a statistically complete bright end of the PNLF consisting of 328 PNs. The data were taken from the corresponding catalog (Méndez et al. 2008a).

On the assumption that the PNLFs of M 31's bulge and NGC 4697 are identical, we adopted the distance modulus $m-M = 30.1$ determined by the PNLF method (Méndez et al. 2001). The extinction correction for λ5007 was 0.105 mag, based on $E(B-V) = 0.03$.

Again using the absorbing factor distribution from the previous section, we fitted our simulated PNLF to the observed one. We found the following best-fitting values: a mass range of 0.530 to 0.580 solar masses and a sample size of 3000 PNs (see Figure 8). Calculating the fit factor r for the three maximum final masses gave us 0.16 for 0.570 $M_\odot$, 0.09 for 0.580 $M_\odot$, and 0.34 for 0.590 $M_\odot$. This time, we got a very clear best fit. The reason for this is the much larger sample size in NGC 4697 compared to that in M 31. We conclude that our new PNLF simulations work very well with a maximum final mass of 0.58 $M_\odot$, confirming a preliminary result by Méndez (2017).

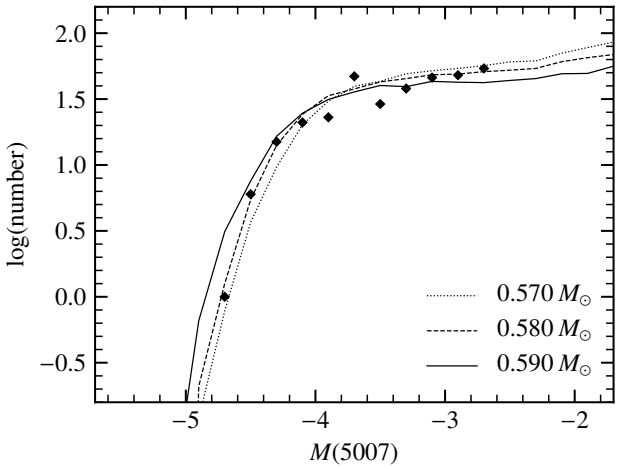

Figure 8. Statistically complete observed PNLF of NGC 4697 (328 PNs) from Méndez et al. (2001). We use a λ5007 extinction correction of 0.105 mag and a distance modulus of $m-M = 30.1$. The data are binned into 0.2 mag intervals. The observed PNLF (diamonds) is compared with simulated PNLFs using the absorbing factor distribution from Figure 6. The sample size for each simulated PNLF is 3000 PNs. The simulations were run with three different mass ranges, from 0.530 $M_\odot$ to the respective maximum final mass displayed at the bottom right.

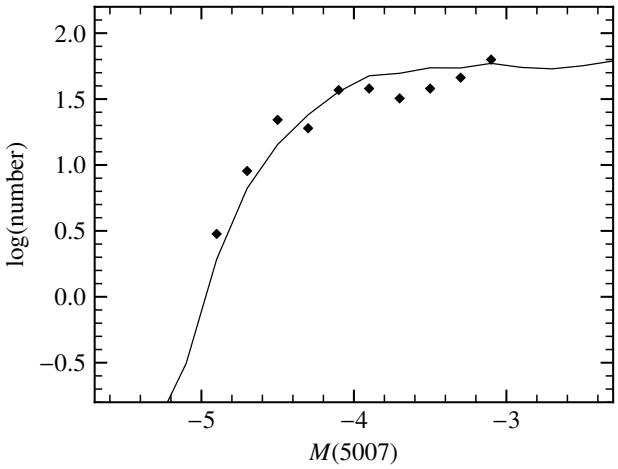

Figure 9. Statistically complete observed PNLF of NGC 4697 (diamonds, 328 PNs) using the same extinction correction 0.105 mag as before, and an SBF distance modulus $m-M = 30.4$ instead of the PNLF distance modulus. In order to fit our simulated PNLF (solid line), we need a maximum final mass of 0.61 $M_\odot$ and a sample size of 5200. The absorbing factor distribution is, as before, from Figure 6.

7. INTERPRETATION OF SBF DISTANCES IN TERMS OF THE MAXIMUM FINAL MASS

The use of the PNLF for distance determinations is based on the assumption that the PNLF's bright end is universal. Any systematic difference between PNLF distances and those determined by other methods is a challenge to that assumption. The SBF method of distance determination (Tonry & Schneider 1988; Tonry et al. 2001; Blakeslee et al. 2009) has shown a tendency to produce larger distance moduli than the PNLF method, by about 0.3 to 0.4 mag (Teodorescu et al. 2010). We refer the reader to Ciardullo (2012) for a discussion of the most likely cause for this systematic effect: zero point errors arising from limited knowledge of internal extinction in the calibrator galaxies, to which the PNLF and SBF methods react in opposite ways. In what follows we would like to illustrate the consequences of assuming that the SBF distances of elliptical galaxies are correct.

An increased distance forces the PNLF to become more luminous. What maximum final mass would be required for our simulated PNLF to fit an observed PNLF if shifted to the SBF distance? Consider for example NGC 4697. Blakeslee et al. (2009) used the SBF method to determine a distance modulus $m - M = 30.491 \pm 0.065$. We adopted an SBF distance as close to the PNLF distance as allowed by the SBF error bars: $m - M = 30.4$. As in Section 6, we used an extinction correction of 0.105 mag. With those numbers we transformed apparent into absolute λ5007 magnitudes. In order to get a fit with our simulated PNLF we needed to increase the maximum final mass to 0.61 $M_\odot$. The sample size also increased to 5200 (see Figure 9). The fit parameter was $r = 0.34$.

As another example we took M 60, an elliptical galaxy in the Virgo Cluster. For the observed data, we used the method described by Teodorescu et al. (2011) to get a statistically complete sample of 218 PNs. We adopted their PNLF distance modulus of $m - M = 30.7$ and extinction factor of 0.09 in our calculations. After fitting the simulated PNLF to the observed one, we got a sample size of 2950 and a maximum final mass of 0.58 $M_\odot$ (see Figure 10). The fit parameter was $r = 0.26$.

Next, we adopted an SBF distance as close to the PNLF distance as allowed by the SBF error bars from Blakeslee et al. (2009): $m - M = 31.0$ (they found $m - M = 31.082 \pm 0.079$) and we recalculated the absolute λ5007 magnitudes. Again, to force a fit with our simulated PNLF, we needed a maximum final mass of 0.61 $M_\odot$ and a sample size of 5350 (see Figure 11). The fit parameter was $r = 0.28$.

A summary of our tests is given in Table 1. In both cases (NGC 4697 and M 60) the PNLF distance leads to a maximum final mass of 0.58 $M_\odot$, whereas the SBF distance leads to 0.61 $M_\odot$. The problem with accepting the SBF distances is, first, that we do not expect such massive central stars to originate from an old stellar population; and second, that the PNs defining the bright end of the PNLF in galaxies like NGC 4697 and M 60 become more luminous than any PNs ever discovered in our Local Group. If SBF distances are confirmed, we will need to find explanations for these anomalies.

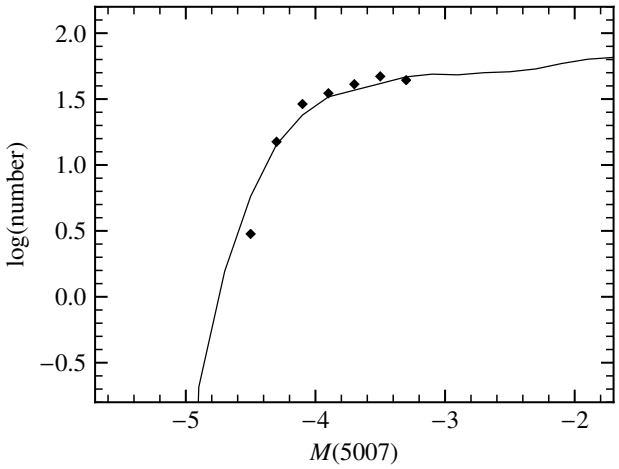

Figure 10. Statistically complete observed PNLF of M 60 (diamonds, 218 PNs) using an extinction correction of 0.09 mag and the PNLF distance modulus of $m - M = 30.7$, compared to our simulated PNLF (solid line) with a maximum final mass of 0.58 $M_\odot$, a sample size of 2950, and the absorbing factor distribution from Figure 6.

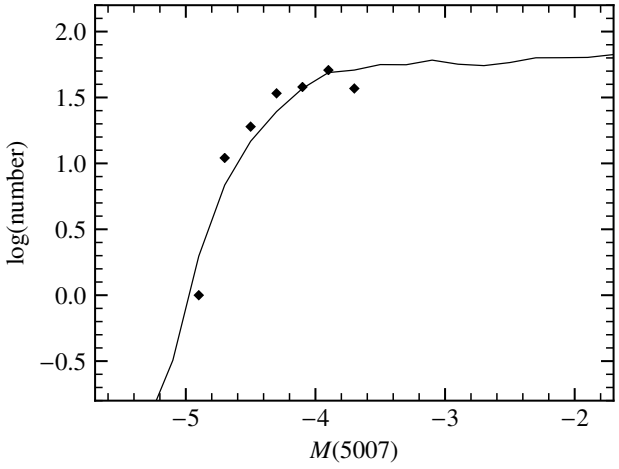

Figure 11. Statistically complete observed PNLF of M 60 (diamonds, 218 PNs) using the same extinction correction 0.09 mag as before, and an SBF distance modulus $m - M = 31.0$ instead of the PNLF distance modulus. In order to fit with our simulated PNLF (solid line), we now need a maximum final mass of 0.61 $M_\odot$ and a sample size of 5350. The absorbing factor distribution is, as before, from Figure 6.

Probably the best way to test SBF and PNLF distances will be to use Tip of the Red Giant Branch (TRGB) distances. The method is described by Makarov et al. (2006); it has been applied to many galaxies up to distances of about 10 Mpc. Ideally, we need at least ten TRGB distances in the Virgo and Fornax clusters to yield a statistically convincing result. This will be possible with the James Webb Space Telescope (JWST), which is expected to allow TRGB distance determinations up to at least 30 Mpc.

Table 1. Values used for PNLF and SBF distances of NGC 4697 and M 60, and the respective best fitting parameters of the simulation. The fit parameter r is defined in Section 5.

	NGC 4697		M 60	
	PNLF	SBF	PNLF	SBF
distance modulus	30.1	30.4	30.7	31.0
extinction correction	0.105	0.105	0.09	0.09
sample size	3000	5200	2950	5350
maximum final mass	0.58	0.61	0.58	0.61
fit parameter	0.09	0.34	0.26	0.28

8. PN FORMATION RATES

A fit to the observed PNLF with our simulated PNLF provides a simultaneous determination of distance modulus and sample size (the total number of PNs in the surveyed area of the galaxy). What is the effect of the new Miller Bertolami tracks on PN formation rates? Having obtained new sample sizes, we can recalculate the specific PN formation rate $\dot{\xi}$ with

$$n_{\rm PN} = \dot{\xi} L_T t_{\rm PN} \quad (1)$$

where $n_{\rm PN}$ is the sample size, L_T is the total luminosity of the sampled population, and $t_{\rm PN} = 30\,000$ yr is the lifetime of a PN. We take L_T from Méndez et al. (2001) for NGC 4697: $L_T = 1.95 \times 10^{10}\,L_\odot$. With the new sample size $n_{\rm PN} = 3000$ from Section 6 we get $\dot{\xi} = 5 \times 10^{-12}\,{\rm yr}^{-1}\,{L_\odot}^{-1}$. This is slightly lower than the earlier result, $\dot{\xi} = 6 \times 10^{-12}\,{\rm yr}^{-1}\,{L_\odot}^{-1}$ (Méndez et al. 2001). It should be noted that the uncertainty is still high at around $\pm 2 \times 10^{-12}\,{\rm yr}^{-1}\,{L_\odot}^{-1}$.

We can perform the same calculation for M 60. The total bolometric luminosity of the sample from Teodorescu et al. (2011), $L_T = 8 \times 10^{10}\,L_\odot$, and the determined sample size $n_{\rm PN} = 2950$ from Section 7 are used to get $\dot{\xi} = 1.2 \times 10^{-12}\,{\rm yr}^{-1}\,{L_\odot}^{-1}$. Again, this is lower than the earlier result, $\dot{\xi} = 1.7 \times 10^{-12}\,{\rm yr}^{-1}\,{L_\odot}^{-1}$ (Teodorescu et al. 2011). The uncertainty is also high for M 60.

Since post-AGB stellar evolution is much faster along the Miller Bertolami tracks than what previous models suggested, one might expect a higher PN formation rate in order to provide the amount of PNs we observe. However, the final mass range has also changed. Since we are using lower final masses, the central stars move much more slowly along their respective tracks in the HR diagram. Ultimately, this leads to a somewhat smaller PN formation rate, just as we can see in our calculations for NGC 4697 and M 60.

9. PNLF SHAPES

Méndez & Soffner (1997) found a change of slope between magnitudes $M(5007) = -3.5$ and -2.3. While our simulations do not entirely eliminate this feature, it is much less noticeable since we no longer have any negative slope in that interval. The PNs in this section of the PNLF are mostly on heating tracks and in the curved section joining the heating and cooling tracks. Comparing our distribution of PNs in the HR diagram (Figure 3) with the one in Figure 2 of Méndez & Soffner (1997), it is clear that we now have a much larger amount of PNs with luminosities immediately below $\log L = 3.5$ in the heating tracks and the curved section. The distribution of PNs in this region of the HR diagram is also more uniform. Therefore, it seems that the lack of such PNs in Méndez & Soffner (1997) had been the reason for the change of slope in the PNLF. This can be traced to the existence of a quick drop in luminosity as the H-burning shell is extinguished and the central star enters the white dwarf cooling track.

It is important to note that all the H-burning central stars show the luminosity drop, but it is more pronounced for the more massive ones (see Figure 1). Thus the adoption of the Miller Bertolami (2016) tracks and substantially lower central star masses leads to predicting a monotonically increasing PNLF for an old population, apparently confirmed by NGC 4697. However, other galaxies, like the LMC and SMC, do show a "camel-shaped" PNLF (Jacoby & De Marco 2002; Reid & Parker 2010a). This kind of shape might be explained by involving slightly more massive central stars, but also by a relative lack of lower-mass stars (see Section 5 of Méndez et al. 2008b). We can test this by applying our PNLF simulations to the LMC.

Reid & Parker (2010a) present a sample of PNs in the LMC over a large range of magnitudes. We used their sample of 577 PNs in the central 25 deg^2 region of the LMC (Tables 1 and 2 in the corresponding catalog, Reid & Parker 2010b). For the transformation into absolute λ5007 magnitudes, we adopted their calculated distance modulus of 18.50 and an extinction correction of 0.46 mag, based on $E(B-V) = 0.13$ (Massey et al. 1995; Soffner et al. 1996).

Fitting the simulated PNLF to the observed one, we found that we can obtain the valley in the PNLF between $M(5007) = -3.5$ and -0.5, similar to what we can see in Reid & Parker (2010a) (see Figure 12). As expected from our earlier discussion, we had to increase both the minimum and maximum final masses to 0.55 and 0.59 to get this "camel shape". Since there are complicating factors in this case (possible differences in the age of the population and in extinction corrections), we do not expect a perfect agreement, but are satisfied that the "camel shape" in the LMC can be reproduced by changing just a few parameters.

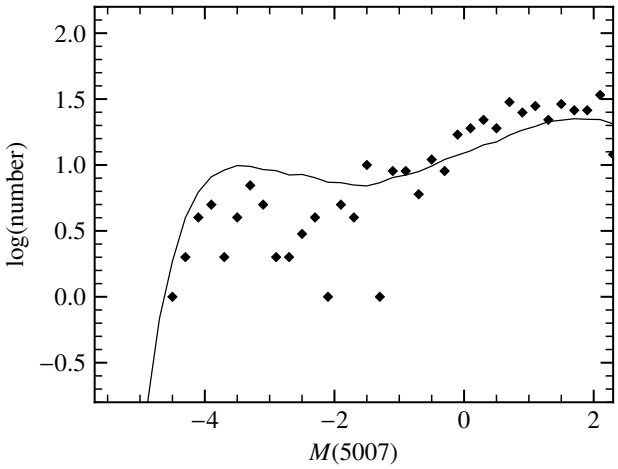

Figure 12. Observed PNLF of the central 25 deg^2 region of the LMC (577 PNs) from Reid & Parker (2010b). We use a λ5007 extinction correction of 0.46 mag and a distance modulus of $m - M = 18.50$. The data are binned into 0.2 mag intervals. The observed PNLF (diamonds) is compared with our simulated PNLF (solid line) with modified central star mass range (0.55 to 0.59 $M_\odot$). The absorbing factor distribution is from Figure 6. The sample size for the simulated PNLF is 600 PNs.

It should be clear that we are far from knowing all the details that contribute to generate the PNLF in any stellar population. To mention just a few, we have the effects of binary evolution and the existence of a minor (but significant) fraction of He-burning central stars in addition to the H-burners. Such complications are very hard to model in Monte Carlo style. However, it is remarkable how the simple PNLF modeling strategy we have used, when combined with the new post-AGB evolutionary tracks by Miller Bertolami, gives a much more consistent explanation of the PNLF than could have been expected 10 years ago.

10. CONCLUSION

We have explored the influence of the new post-AGB evolutionary tracks by Miller Bertolami on the interpretation of the observed PNLFs in other galaxies. For that purpose we have revised an earlier procedure for numerical PNLF simulations (Méndez & Soffner 1997). Only small adjustments to several routines were made, without altering the basic philosophy of the method, which is to rely on empirical information about nebular and stellar properties. A comparison of our simulations with the observed PNLF of M 31's bulge, whose distance is very well known, shows that we need to allow for optically thin PNs. Having established the distribution of absorbing factors μ with M 31, we selected a galaxy with a larger sample size, NGC 4697, to get a better estimate for the maximum final mass. We briefly illustrate the consequences of adopting SBF distances, as a way of remarking on the importance of solving the discrepancy between PNLF and SBF

distances. We also report on the effect of the new evolutionary tracks on the calculation of PN formation rates. Finally, we show that by adjusting the minimum final mass that leads to a visible PN, we can reproduce the "camel shape" exhibited by PNLFs in the Magellanic Clouds.

ACKNOWLEDGMENTS

We thank M. M. Miller Bertolami for making his evolutionary track data available to us. L.M.V. acknowledges partial support from the German Academic Scholarship Foundation and would like to thank the Institute for Astronomy, University of Hawaii at Manoa, for their kind hospitality during the course of this research.

REFERENCES

Blakeslee, J. P., Jordán, A., Mei, S., et al. 2009, ApJ, 694, 556, doi: 10.1088/0004-637X/694/1/556

Ciardullo, R. 2012, Ap&SS, 341, 151, doi: 10.1007/s10509-012-1061-2

Ciardullo, R., Jacoby, G. H., Ford, H. C., & Neill, J. D. 1989, ApJ, 339, 53, doi: 10.1086/167275

Cummings, J. D. 2017, in Planetary Nebulae: Multi-Wavelength Probes of Stellar and Galactic Evolution, Vol. 323, 157–164

Gesicki, K., Zijlstra, A. A., & Miller Bertolami, M. M. 2018, Nature Astronomy, 52, doi: 10.1038/s41550-018-0453-9

Jacoby, G. H. 1989, ApJ, 339, 39, doi: 10.1086/167274

Jacoby, G. H., & Ciardullo, R. 1999, ApJ, 515, 169, doi: 10.1086/307024

Jacoby, G. H., & De Marco, O. 2002, AJ, 123, 269, doi: 10.1086/324737

Kepler, S. O., Koester, D., Romero, A. D., Ourique, G., & Pelisoli, I. 2017, in 20th European White Dwarf Workshop, Vol. 509, 421

Makarov, D., Makarova, L., Rizzi, L., et al. 2006, AJ, 132, 2729, doi: 10.1086/508925

Massey, P., Lang, C. C., Degioia-Eastwood, K., & Garmany, C. D. 1995, ApJ, 438, 188, doi: 10.1086/175064

Méndez, R. H. 2017, in Planetary Nebulae: Multi-Wavelength Probes of Stellar and Galactic Evolution, Vol. 323, 298–302

Méndez, R. H., Kudritzki, R. P., Ciardullo, R., & Jacoby, G. H. 1993, A&A, 275, 534

Méndez, R. H., Kudritzki, R. P., & Herrero, A. 1992, A&A, 260, 329

Méndez, R. H., Riffeser, A., Kudritzki, R. P., et al. 2001, ApJ, 563, 135, doi: 10.1086/323794

Méndez, R. H., & Soffner, T. 1997, A&A, 321, 898

Méndez, R. H., Teodorescu, A. M., & Kudritzki, R. P. 2008a, The Astrophysical Journal Supplement Series, 175, 522, doi: 10.1086/524683

Méndez, R. H., Teodorescu, A. M., Schönberner, D., Jacob, R., & Steffen, M. 2008b, ApJ, 681, 325, doi: 10.1086/588808

Méndez, R. H., Thomas, D., Saglia, R. P., et al. 2005, ApJ, 627, 767, doi: 10.1086/430498

Miller Bertolami, M. M. 2016, A&A, 588, A25, doi: 10.1051/0004-6361/201526577

Reid, W. A., & Parker, Q. A. 2010a, MNRAS, 405, 1349, doi: 10.1111/j.1365-2966.2010.16635.x

—. 2010b, VizieR Online Data Catalog, J/MNRAS/405/1349

Soffner, T., Méndez, R. H., Jacoby, G. H., et al. 1996, A&A, 306, 9

Teodorescu, A. M., Méndez, R. H., Bernardi, F., Riffeser, A., & Kudritzki, R. P. 2010, ApJ, 721, 369, doi: 10.1088/0004-637X/721/1/369

Teodorescu, A. M., Méndez, R. H., Bernardi, F., et al. 2011, ApJ, 736, 65, doi: 10.1088/0004-637X/736/1/65

Tonry, J., & Schneider, D. P. 1988, AJ, 96, 807, doi: 10.1086/114847

Tonry, J. L., Dressler, A., Blakeslee, J. P., et al. 2001, ApJ, 546, 681, doi: 10.1086/318301